

# HOTFLoc++: End-to-End Hierarchical LiDAR Place Recognition, Re-Ranking, and 6-DoF Metric Localisation in Forests

Ethan Griffiths<sup>\*†§</sup>, Maryam Haghighat<sup>†</sup>, Simon Denman<sup>†</sup>, Clinton Fookes<sup>†</sup> and Milad Ramezani<sup>\*</sup>

**Abstract**—This article presents HOTFLoc++, an end-to-end framework for LiDAR place recognition, re-ranking, and 6-DoF metric localisation in forests. Leveraging an octree-based transformer, our approach extracts hierarchical local descriptors at multiple granularities to increase robustness to clutter, self-similarity, and viewpoint changes in challenging scenarios, including ground-to-ground and ground-to-aerial in forest and urban environments. We propose a learnable multi-scale geometric verification module to reduce re-ranking failures in the presence of degraded single-scale correspondences. Our coarse-to-fine registration approach achieves comparable or lower localisation errors to baselines, with runtime improvements of two orders of magnitude over RANSAC for dense point clouds. Experimental results on public datasets show the superiority of our approach compared to state-of-the-art methods, achieving an average Recall@1 of 90.7% on CS-Wild-Places: an improvement of 29.6 percentage points over baselines, while maintaining high performance on single-source benchmarks with an average Recall@1 of 91.7% and 96.0% on Wild-Places and MulRan, respectively. Our method achieves under 2m and 5° error for 97.2% of 6-DoF registration attempts, with our multi-scale re-ranking module reducing localisation errors by  $\sim 2\times$  on average. The code will be available upon acceptance.

## I. INTRODUCTION

Place Recognition (PR) and metric localisation are fundamental for long-term mobile robot autonomy in GPS-denied environments, yet most existing methods are tailored to structured indoor or urban environments and struggle to generalise to natural settings such as forests. These environments lack distinctive, persistent landmarks and instead exhibit strong self-similarity, clutter and seasonal variability, which undermine both keypoint-based matching and single-scale geometric verification. These problems are exacerbated in cross-source settings, where data is captured from two differing viewpoints or sensors (*i.e.*, ground *vs.* aerial), causing low scene overlap and distribution shifts.

Typically, 6-DoF re-localisation in large-scale environments follows a two-step process: 1) retrieval-based PR (*i.e.*, coarse localisation), and 2) 6-DoF pose estimation between the query and top place candidate. Due to the necessity of retrieving high quality candidates to ensure successful registration, re-ranking is often employed to filter erroneous retrievals [1]. In the point cloud domain, geometric consistency has proven a strong prior for verifying retrieval

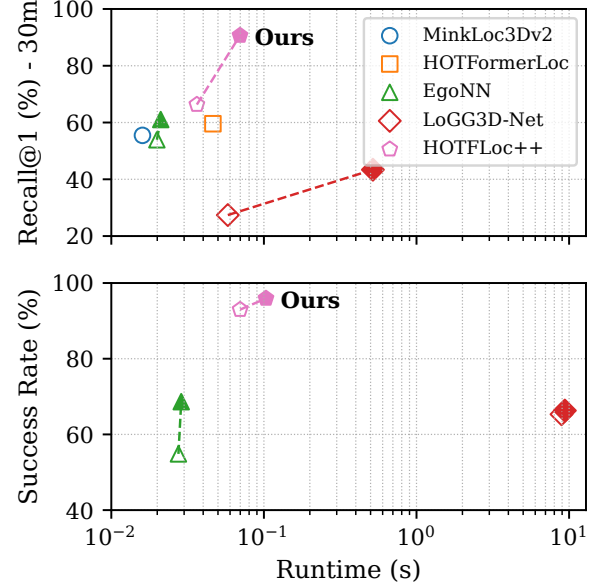


Fig. 1: HOTFLoc++ achieves Pareto-optimality for place recognition (top) and metric localisation (bottom) on CS-Wild-Places. Filled symbols denote results after re-ranking.

quality. However, current approaches evaluate it only at a fine-grained level. This is insufficient in complex and cross-domain scenarios where keypoints at a single scale fail to capture hierarchical structures in the data that can address the inherent ambiguity of homogeneous scenes. In cross-source settings, single-scale features are more prone to degradations than multi-scale features [2], further harming robustness.

On the other hand, existing approaches for 6-DoF re-localisation typically rely on salient keypoint detection, which struggles to produce repeatable keypoints in repetitive or cluttered environments [3], or requires robust solvers to find local feature correspondences, which are often too slow for real-time deployment. We argue that in such environments, multi-scale feature fusion is essential to maximise extracted information and improve robustness to aliasing, occlusion and seasonal change.

To this end, we propose HOTFLoc++, a unified and hierarchical end-to-end network for LiDAR PR, re-ranking, and 6-DoF metric localisation. We leverage the hierarchical features of HOTFormerLoc [4] to train a multi-scale geometric verification (MSGV) module that analyses geometric consistency at multiple feature granularities to choose the best candidate for re-localisation. Our keypoint-free re-localisation module then leverages the octree hierarchy of HOTFormerLoc to process features in a coarse-to-fine approach by selecting

<sup>\*</sup>CSIRO Robotics, Data61, CSIRO, Brisbane, Australia. E-mails: [firstname.lastname@data61.csiro.au](mailto:firstname.lastname@data61.csiro.au)

<sup>†</sup>School of Electrical Engineering and Robotics, Queensland University of Technology (QUT), Brisbane, Australia. E-mails: [{maryam.haghighat, s.denman, c.fookes}@qut.edu.au](mailto:{maryam.haghighat, s.denman, c.fookes}@qut.edu.au)

<sup>§</sup>Corresponding author

likely patch correspondences and estimating the patch-wise 6-DoF registration which maximises the global inlier set. Importantly, we achieve low registration errors without relying on robust solvers such as RANSAC, with over two orders of magnitude faster inference on dense point clouds. Our robust hierarchical pipeline achieves significant performance gains on challenging natural environment datasets (Fig. 1), while retaining high performance on urban datasets, as demonstrated by our extensive experiments. Notably, we show that jointly training for PR, re-ranking, and re-localisation improves the downstream performance of PR compared to single-task training, due to the complementary constraints imposed by our re-ranking and re-localisation losses.

Our contributions include (a) HOTFLoc++, an end-to-end pipeline for place recognition, re-ranking, and 6-DoF metric localisation that achieves an optimal trade-off of performance and efficiency, (b) MSGV, a learnable re-ranking approach that leverages multi-scale correspondences to enhance robustness to single-scale feature degradations, (c) Extensive experiments and comparisons with state-of-the-art baselines, demonstrating the effectiveness of the proposed framework.

## II. RELATED WORKS

### A. LiDAR Place Recognition

LiDAR place recognition (LPR) is typically formulated as a retrieval problem, where point clouds are encoded into descriptors to be queried from a database. Prior to deep learning approaches, handcrafted descriptors [5], [6] were common, but have since been superseded by methods trained via metric learning. These utilise three main types of feature encoder: PointNet [7], [8], Sparse CNNs [9]–[13], and transformers [4], [14]–[16]. Sparse CNN methods outperformed early transformer methods in speed and accuracy [11], [13], but recent approaches have bridged this gap [4], [16].

However, most LPR research has focused on urban environments, while research into unstructured natural environments has lagged. Wild-Places [17] released the first large-scale dataset for long-term LPR in forests, identifying the domain gap challenging existing SOTA models. Cross-source PR has also lagged, with recent works like CrossLoc3D [2] exploring ground-to-aerial LPR in campus environments. HOTFormerLoc [4] proposed CS-Wild-Places: an aerial extension to Wild-Places, and demonstrated the effectiveness of hierarchical transformers in single- and cross-source settings.

### B. Metric Localisation

Existing approaches for unified LPR and 6-DoF metric localisation typically fall into two categories: (a) sparse keypoint-based [8], [13], or (b) dense correspondence-based [10], [16]. Sparse keypoint methods such as EgoNN [13] predict a keypoint saliency map to filter uncertain keypoints, with RANSAC [18] for subsequent pose estimation. This works well in environments with distinct geometric features, but keypoint repeatability suffers in unstructured and cluttered environments [3]. Dense approaches typically apply robust solvers to local feature correspondences which incurs high computational cost, especially

with poor initial correspondences. LCDNet [10] employs an Unbalanced Optimal Transport (UOT) head with weighted SVD to efficiently estimate 6-DoF pose during training, but relies on RANSAC at inference for better robustness.

Recent works in point cloud registration have explored more sophisticated end-to-end approaches. Deep robust estimators such as PointDSC [19] aim to be drop-in replacements for RANSAC, training a small network with a spatial consistency prior to predict outlier correspondences. CoFiNet [20] and GeoTransformer [21] adopt keypoint-free coarse-to-fine registration schemes, which utilise patch-level correspondences to improve robustness in low-overlap scenes. We demonstrate that coarse-to-fine registration is better suited to unstructured environments and cross-source scenarios than keypoint-based methods.

### C. Re-Ranking

SpectralGV (SGV) [1] is the pioneering method for geometric verification re-ranking in LPR. Leveraging a spectral technique to capture spatial consistency of correspondences, it achieves sub-linear time complexity with comparable performance to RANSAC-based geometric verification. However, SGV only considers correspondences at a fixed feature granularity, lacking adaptiveness in the presence of degraded correspondences. We propose a learnable alternative that jointly considers the spatial consistency of multi-scale correspondences, improving robustness when a single feature resolution is not sufficient to determine correspondences. Such scenarios can occur when traversing between environments with varying geometric properties (*e.g.*, urban to forest), or in cross-source settings as observed in [2].

## III. METHOD

In this section, we detail our proposed HOTFLoc++ for end-to-end LiDAR PR (LPR), re-ranking, and 6-DoF metric localisation. Our entire pipeline is depicted in Fig. 2.

### A. Place Recognition with Hierarchical Features

We formulate place recognition as a retrieval problem. Let  $\mathcal{Q} = \{\mathbf{q}_i \in \mathbb{R}^3\}_{i=1}^N$  be a query point cloud with  $N$  points captured by a LiDAR sensor. Let  $\mathcal{D} = \{\mathcal{P}_1, \dots, \mathcal{P}_M\}$  be a database of  $M$  point clouds captured in a prior session, where  $\mathcal{P}_i = \{\mathbf{p}_j \in \mathbb{R}^3\}_{j=1}^{N_i}$  and  $N_i$  is variable for each point cloud. In LPR, the goal is to retrieve point cloud  $\mathcal{P}_i \in \mathcal{D}$  which represents the same place as  $\mathcal{Q}$ , ideally with as much overlap as possible. We employ HOTFormerLoc [4] as our place recognition backbone, which leverages an octree-based hierarchical transformer to extract strong multi-scale local features. These are pooled with a pyramid attentional pooling layer to produce a robust global descriptor. As we demonstrate in Sec. IV, multi-scale features are essential for ensuring robustness of re-ranking and metric localisation.

Formally, our backbone encoder (Fig. 2a) learns a function  $f_\theta$ , parametrised by  $\theta$ , that maps a point cloud to a set of multi-scale local features and a global descriptor

$$f_\theta : \mathcal{P} \rightarrow (\mathcal{F}, \mathbf{d}_G), \quad \mathcal{F} = [F_1, \dots, F_S] \quad (1)$$

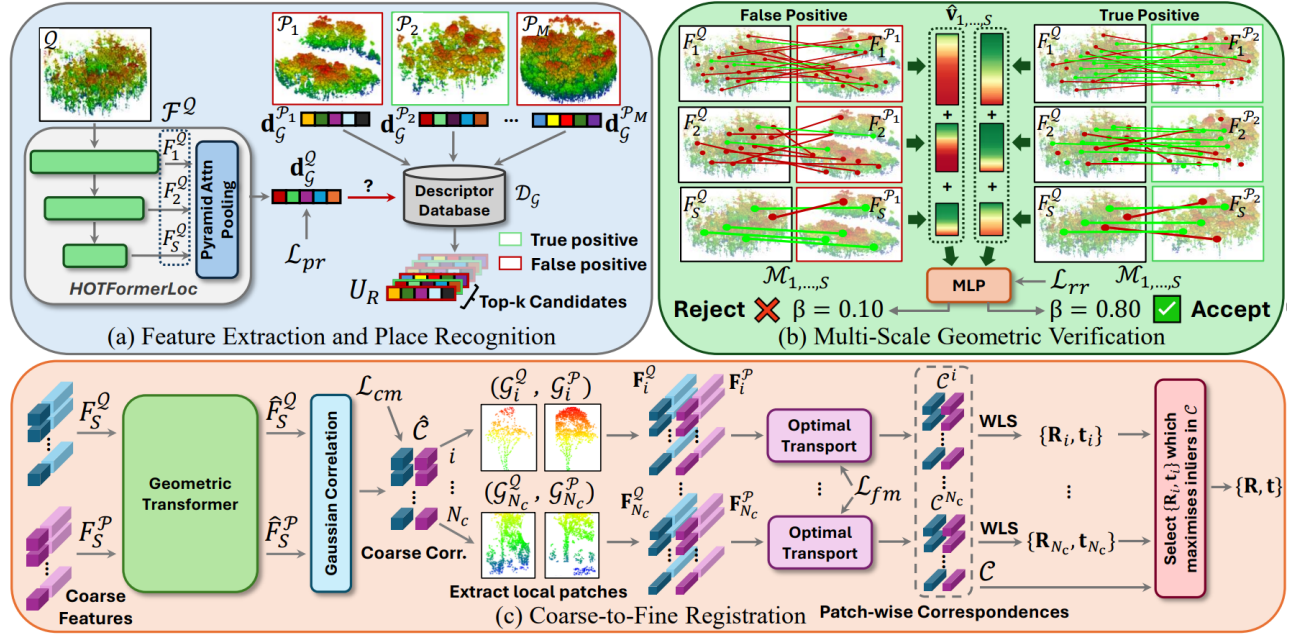


Fig. 2: Pipeline of HOTFLoc++. (a) We use an octree-based transformer backbone [4] to extract multi-scale local features and a robust global descriptor for place recognition. (b) Our learnable Multi-Scale Geometric Verification module re-ranks retrievals, improving robustness to degraded or erroneous single-resolution correspondences. (c) Our coarse-to-fine registration extracts patch-level correspondences and refines the patch-wise registration which maximises the global inlier ratio.

where  $F_s = \{\mathbf{d}_{s,i} \in \mathbb{R}^{d_s}\}_{i=1}^{K_s}$  is a set of  $K_s$  local descriptors of dimension  $d_s$  from level  $s \in \{1, \dots, S\}$  of the feature pyramid, which are aggregated into a  $d$ -dimensional global descriptor  $\mathbf{d}_G \in \mathbb{R}^d$  via pyramid attention pooling [4].

During inference, the global descriptor  $\mathbf{d}_G^Q$  of query  $Q$  is matched with a pre-computed database of descriptors  $\mathcal{D}_G$  to obtain the top- $k$  retrieval candidates  $U_R = [\mathcal{P}_{R_1}, \dots, \mathcal{P}_{R_k}]$ , ordered by similarity to the query descriptor.

### B. Learnable Multi-Scale Geometric Verification

Using compact global descriptors for retrieval enables fast inference in large-scale environments, but inevitably produces false positives in ambiguous or aliased scenes. Re-ranking addresses this by analysing the local descriptors of the top- $k$  retrieval candidates in  $U_R$ , and re-ordering them based on a fitness score, producing  $U_{RR} = [\mathcal{P}_{RR_1}, \dots, \mathcal{P}_{RR_k}]$ . In particular, geometric consistency (GC) re-ranking methods such as SpectralGV (SGV), which exploit the spatial consistency of local feature correspondences, have proven to be robust and effective for LPR [1], [22]. However, existing GC approaches only consider a single feature granularity, and handcrafted approaches such as [1] require further work to integrate multi-scale correspondences. We argue this limitation reduces the effectiveness of GC-based re-ranking when features of one resolution are degraded, which can occur in cross-source PR settings [2].

We propose a learnable re-ranking method, coined Multi-Scale Geometric Verification (MSGV), that considers geometric consistency at multiple feature granularities (Fig. 2b). Consider query point cloud  $Q$  and retrieval candidate  $\mathcal{P} \in U_R$ , with corresponding multi-scale local features  $\mathcal{F}^Q$  and  $\mathcal{F}^P$ . For each  $F_s^Q \in \mathcal{F}^Q$  and  $F_s^P \in \mathcal{F}^P$ , we process all local features with a small MLP and construct a set of putative

correspondences via nearest-neighbour matching

$$\mathcal{M}_s = \{(\mathbf{q}_s^{(i)}, \mathbf{p}_s^{(i)})\}_{i=1}^{\lambda_s} \quad (2)$$

where only the top- $\lambda_s$  matches are kept, and  $\mathbf{q}_s^{(i)}$  and  $\mathbf{p}_s^{(i)}$  denote the centroids of the matched features at level  $s$ . We capture the pairwise length consistency between correspondences with a geometric consistency matrix  $\mathbf{M}_s \in \mathbb{R}^{\lambda_s \times \lambda_s}$ , with entries  $m_{i,j} \in \mathbf{M}_s$  defined as

$$m_{i,j} = \left[ 1 - \frac{\sigma_{i,j}^2}{\sigma_d^2} \right]_+, \quad \sigma_{i,j} = \left| \|\mathbf{q}_s^{(i)} - \mathbf{q}_s^{(j)}\|_2 - \|\mathbf{p}_s^{(i)} - \mathbf{p}_s^{(j)}\|_2 \right| \quad (3)$$

where  $[\cdot]_+ = \max(\cdot, 0)$ , and  $\sigma_d$  is a distance threshold controlling sensitivity to length difference.

As observed in [23], the values of the leading eigenvector  $\mathbf{v}_s$  of  $\mathbf{M}_s$  can be considered as the association of each correspondence with the main cluster of  $\mathbf{M}_s$ , and can thus be interpreted as inlier probabilities. This is robust in the presence of outliers as the main cluster of  $\mathbf{M}_s$  is statistically formed by correct correspondences, and the likelihood of outliers forming a spatially consistent cluster is low.

To seamlessly integrate the spatial consistency of our multi-scale features into a scalar fitness value, we compute  $\mathbf{v}_s$  for all  $s \in \{1, \dots, S\}$  and process the concatenated vectors with an MLP to produce the fitness score  $\beta \in [0, 1]$ . Inspired by GeoAdapt [22], we aid the MLP optimisation by using  $\hat{\mathbf{v}}_s$  instead of the raw leading eigenvectors, where  $\hat{\mathbf{v}}_s$  is  $\mathbf{v}_s$  with values sorted and min-max normalised into the range  $[0, 1]$ . This process is computed in parallel for all  $\mathcal{P} \in U_R$ , ensuring MSGV remains efficient as the number of candidates  $k$  increases. Finally,  $U_R$  is arranged in decreasing order of the  $\beta$  scores to produce re-ranked candidates  $U_{RR}$ .



### C. Coarse-to-Fine Registration

Following PR and re-ranking success, we obtain the top-candidate point cloud  $\mathcal{P}$  which overlaps query  $\mathcal{Q}$ . Our goal is to estimate a rigid transformation  $\mathbf{T} = \{\mathbf{R}, \mathbf{t}\}$  which registers  $\mathcal{Q}$  and  $\mathcal{P}$ , with 3D rotation  $\mathbf{R} \in SO(3)$  and translation  $\mathbf{t} \in \mathbb{R}^3$ . Existing approaches typically estimate  $\mathbf{T}$  with RANSAC [18], matching dense local features [11], [16], or a set of sparse keypoints [10], [13]. However, computing RANSAC on thousands of local features (as is the case for dense LiDAR scans) is infeasible for real-time performance. EgoNN avoids this issue by using a small set of keypoints, but is prone to extracting degenerate keypoints in cluttered and unstructured environments such as forests, where dense foliage and a lack of distinct landmarks harm repeatability [3]. Furthermore, as  $\mathbf{T}$  is estimated using sparse keypoints, ICP is often needed to ensure a tight registration.

By contrast, we adopt a keypoint-free coarse-to-fine registration approach that enables efficient and robust correspondence prediction with low registration errors. Importantly, we estimate 6-DoF poses via a patch-to-patch registration scheme (Fig. 2c), as opposed to keypoint-to-keypoint.

Given the pre-computed multi-scale local features  $\mathcal{F}^{\mathcal{Q}}$  and  $\mathcal{F}^{\mathcal{P}}$ , we first enhance  $F_S^{\mathcal{Q}}$  and  $F_S^{\mathcal{P}}$  from the coarsest level  $S$  of our feature pyramid with a Geometric Transformer [21] and  $L_2$  normalise them to produce  $\hat{F}_S^{\mathcal{Q}}$  and  $\hat{F}_S^{\mathcal{P}}$ . This lightweight network leverages geometric self-attention and cross-attention layers to explicitly encode intra-point cloud geometric structures and capture inter-point cloud geometric consistency, improving the transformation-invariance of the coarse features. We then establish a set of coarse correspondences  $\hat{\mathcal{C}}$  by computing a Gaussian correlation matrix  $\mathbf{G} \in \mathbb{R}^{|\hat{F}_S^{\mathcal{Q}}| \times |\hat{F}_S^{\mathcal{P}}|}$  [21] between the features. We further perform dual-normalisation on the rows and columns of  $\mathbf{G}$  to suppress ambiguous matches, and finally select the largest  $N_c$  entries in  $\mathbf{G}$  as our coarse correspondences  $\hat{\mathcal{C}}$ .

We consider each coarse correspondence  $\hat{\mathcal{C}}_i \in \hat{\mathcal{C}}$  as a pair of *superpoints* to be matched. This formulation allows us to leverage the fine-grained features from HOTFormerLoc’s feature hierarchy which capture higher frequency detail, enabling more robust matching than with coarse keypoints. Utilising the octree structure of HOTFormerLoc, we expand each coarse correspondence to a patch-level correspondence by assigning the local features  $F_1^{\mathcal{Q}}$  and centroids  $\mathcal{Q}_1$  from the finest level  $1 \in \{1, \dots, S\}$  of the feature pyramid to their parent nodes in the octree at level  $S$

$$\mathcal{G}_i^{\mathcal{Q}} = \{\mathbf{q}_1^{(j)} \in \mathcal{Q}_1 \mid \text{parent}(j) = i\}, i \in \{1, \dots, N_c\} \quad (4)$$

where  $\text{parent}(\cdot)$  maps each fine octant centroid  $\mathbf{q}_1^{(j)}$  to its coarse parent node  $\mathbf{q}_S^{(i)} \in \mathcal{Q}_S$  at level  $S$ . The corresponding fine feature matrix is denoted as  $\mathbf{F}_i^{\mathcal{Q}} \in \mathbb{R}^{|\mathcal{G}_i^{\mathcal{Q}}| \times d_1}$ , where  $d_1$  is the local feature dimension at level 1. Equation (4) is repeated for point cloud  $\mathcal{P}$  to produce patches  $\mathcal{G}^{\mathcal{P}} = \{\mathcal{G}_i^{\mathcal{P}}\}_{i=1}^{N_c}$ , each with corresponding features  $\mathbf{F}_i^{\mathcal{P}} \in \mathbb{R}^{|\mathcal{G}_i^{\mathcal{P}}| \times d_1}$ .

For each patch correspondence  $\hat{\mathcal{C}}_i = (\mathcal{G}_i^{\mathcal{Q}}, \mathcal{G}_i^{\mathcal{P}})$ , we initialise a cost matrix

$$\mathbf{C}_i = \frac{\mathbf{F}_i^{\mathcal{Q}}(\mathbf{F}_i^{\mathcal{P}})^T}{\sqrt{d_1}}, \mathbf{C}_i \in \mathbb{R}^{|\mathcal{G}_i^{\mathcal{Q}}| \times |\mathcal{G}_i^{\mathcal{P}}|} \quad (5)$$

which we append with a dustbin row and column filled with learnable parameter  $\alpha$  to handle unmatched points. We process  $\mathbf{C}_i$  with the learnable Sinkhorn algorithm proposed in [24] to solve the optimal transport (OT) between patches, producing soft assignment matrix  $\bar{\mathbf{Z}}_i$ . We drop the dustbin to obtain  $\mathbf{Z}_i$  as the confidence matrix of correspondences between  $\mathcal{G}_i^{\mathcal{Q}}$  and  $\mathcal{G}_i^{\mathcal{P}}$ . To reduce the impact of erroneous correspondences, we filter out matches with confidence  $z_j^i \in \mathbf{Z}_i$  less than threshold  $\gamma_z$  and select fine correspondences  $\mathcal{C}_i$  through mutual top- $k$  selection on  $\mathbf{Z}_i$ . Finally, we combine the fine correspondences computed for each superpoint pair into a global set of dense correspondences  $\mathcal{C} = \bigcup_{i=1}^{N_c} \mathcal{C}_i$ .

To estimate  $\mathbf{T}$ , we adopt a local-to-global registration (LGR) scheme [21]. It follows a hypothesise-and-verify approach, where a transformation candidate  $\mathbf{T}_i$  is proposed for each superpoint match using its fine-grained correspondences

$$\mathbf{R}_i, \mathbf{t}_i = \min_{\mathbf{R}, \mathbf{t}} \sum_{(\mathbf{q}_j, \mathbf{p}_j) \in \mathcal{C}_i} z_j^i \|\mathbf{R} \cdot \mathbf{q}_j + \mathbf{t} - \mathbf{p}_j\|_2^2 \quad (6)$$

which we solve in closed form with Weighted Least Squares (WLS). Then, we select the transformation  $(\mathbf{R}_i, \mathbf{t}_i)$  with the highest inlier ratio over the global dense correspondence set

$$\mathbf{R}, \mathbf{t} = \max_{\mathbf{R}, \mathbf{t}} \sum_{(\mathbf{q}_j, \mathbf{p}_j) \in \mathcal{C}} \left[ \|\mathbf{R} \cdot \mathbf{q}_j + \mathbf{t} - \mathbf{p}_j\|_2 < \tau_a \right] \quad (7)$$

where  $[\cdot]$  denotes the Iverson bracket, and  $\tau_a$  is the inlier acceptance radius. This process is repeated  $N_r$  times with the surviving inliers by iteratively solving Eqs. (6) and (7) to produce the final estimated transformation  $\mathbf{T}$ .

### D. End-to-End Training

A key advantage of our holistic approach is that we jointly optimise our network for place recognition, re-ranking, and 6-DoF metric localisation at once in our end-to-end training protocol. We argue that these three tasks are complementary, and that jointly optimising all three improves convergence by introducing useful constraints on the features learned by the network. We validate this quantitatively in Sec. IV-E.

To train our entire pipeline end-to-end, the overall loss is formulated as  $\mathcal{L} = \mathcal{L}_{pr} + \lambda_{rr}\mathcal{L}_{rr} + \lambda_{cm}\mathcal{L}_{cm} + \lambda_{fm}\mathcal{L}_{fm}$ , which we detail in the following sections.

*Place Recognition:* We train our PR head in a two-stage manner. In the first stage, we disable the re-ranking and re-localisation heads and train purely on the PR task, using the Truncated Smooth Average Precision (TSAP) loss defined in [12] as  $\mathcal{L}_{pr}$  with a large batch size. Empirically, we find this pre-training provides a stronger initialisation for the HOTFormerLoc backbone, producing better performance.

In the second stage, we enable re-ranking and re-localisation and continue to train with PR enabled. However, we observe that using large PR batches in this stage overpowers the gradients of the other losses, leading to poor overall convergence. Instead, we reduce the PR batch size and swap the TSAP loss for a batch-hard triplet margin loss [25] which performs better for smaller batch sizes [12].

TABLE I: Details of training and evaluation sets. SS and CS denote single-source and cross-source datasets, respectively.

| Dataset             | Split             | Num. Submaps |       |                     |
|---------------------|-------------------|--------------|-------|---------------------|
|                     |                   | Train        | Query | Database            |
| <i>Forest</i> – CS: | Karawatha         | 37,373       | 9,549 | 17,792              |
| CS-Wild-Places [4]  | Venman            | 26,807       | 6,398 | 12,383              |
|                     | QCAT              | —            | 753   | 369                 |
|                     | Samford           | —            | 1,309 | 4,528               |
| <i>Forest</i> – SS: | Karawatha         | 13,661       | 9,642 | 39,847 <sup>†</sup> |
| Wild-Places [17]    | Venman            | 5,435        | 6,395 | 23,472 <sup>†</sup> |
| <i>Urban</i> – SS:  | Sejong (01/02)    | 35,871       | 3,453 | 3,764               |
| MulRan [26]         | DCC (01/02)       | —            | 307   | 469                 |
|                     | Riverside (01/02) | —            | 470   | 603                 |

<sup>†</sup> Cumulative size of databases from all sequences.

*Re-Ranking:* To efficiently train MSGV alongside the PR head, we use a subset of batch-hard triplets mined from PR batches. Specifically, we sort triplets by global descriptor distance of anchor and negative and sample the top- $N_{rr}$  hardest triplets to ensure our re-ranking module learns to distinguish challenging false-positive retrievals. We employ binary cross-entropy (BCE) loss to train the module

$$\mathcal{L}_{rr} = -(y \cdot \log \beta + (1 - y) \log(1 - \beta)) \quad (8)$$

where  $\beta$  is the fitness score predicted by MSGV, and  $y$  is 1 for a positive pair and 0 for negative pairs.

*Coarse-to-Fine Registration:* To train our coarse-to-fine registration head, we employ a second training substep after computing and backpropagating the losses for PR and re-ranking. This frees up GPU memory from intermediate activations and gradients, allowing for larger batch sizes. In this substep, we sample pairs of overlapping point clouds, omitting negatives as they are not required for training metric localisation. We utilise two loss functions to jointly optimise the quality of both coarse and fine correspondences.

To optimise coarse correspondences, we employ an Overlap-Aware Circle Loss [21], which provides better gradients for optimisation than typical cross-entropy and improves matching of low-overlap patches by re-weighting the loss with the proportion of patch overlap. We compute this loss in both directions from  $\mathcal{Q} \rightarrow \mathcal{P}$  and  $\mathcal{P} \rightarrow \mathcal{Q}$  to produce the final loss  $\mathcal{L}_{cm} = (\mathcal{L}_{cm}^{\mathcal{Q}} + \mathcal{L}_{cm}^{\mathcal{P}})/2$ .

To optimise the fine correspondences, we follow Super-Glue [24] and apply the negative log-likelihood loss on the OT assignment matrix  $\bar{\mathbf{Z}}_i$  of each superpoint correspondence  $\hat{\mathcal{C}}_i \in \hat{\mathcal{C}}$ , averaging over all superpoint correspondences to produce  $\mathcal{L}_{fm}$ . During training, we sample ground-truth superpoint correspondences instead of using predicted correspondences to ensure patches have suitable overlap.

## IV. EXPERIMENTS

### A. Datasets and Evaluation Protocol

We train and evaluate HOTFLoc++ on three datasets: CS-Wild-Places [4], Wild-Places [17], and MulRan [26], to demonstrate the effectiveness of our approach in a diverse range of environments and scenes. See Tab. I for details of the training and evaluation sets used for each dataset.

For CS-Wild-Places, we follow the training and evaluation splits proposed in HOTFormerLoc [4] with K-01 and K-02 test regions for validation, but we downsample submaps

TABLE II: HOTFLoc++ hyperparameters per dataset.

| Hyperparameter    | CS-Wild-Places     | Wild-Places        | MulRan             |
|-------------------|--------------------|--------------------|--------------------|
| Learning Rate     | $8 \times 10^{-4}$ | $3 \times 10^{-4}$ | $8 \times 10^{-4}$ |
| Octree Attn. Type | Cartesian          | Cylindrical        | Cartesian          |
| $\sigma_d$        | 5.0 m              | 1.6 m              | 0.4 m              |
| $\tau_a$          | 1.6 m              | 1.6 m              | 0.6 m              |

with a voxel size of 0.4 m instead of 0.8 m, producing an average of 62 k points per submap. For Wild-Places, we use the training split described in [17], and follow the inter-sequence evaluation protocol in our experiments. For MulRan, we follow the Sejong and DCC splits reported in SpectralGV [1], as well as Riverside 01 and 02 with submaps sampled every 10 m along each trajectory. Only Sejong is used for training and validation, allowing unseen evaluation on DCC and Riverside. In all MulRan regions, sequence 01 forms the database, and sequence 02 forms the queries.

To evaluate place recognition, we compute the similarity between the global descriptors of each query and the database and collect the top-k retrieval candidates. We report the Recall@ $k$  (R $k$ ) metric for  $k \in \{1, 5\}$ , defined as the percentage of queries where at least one top-k candidate is within a  $r$ -metre retrieval threshold of the query. We adopt the retrieval thresholds used in previous works, with  $r = 3$  m for Wild-Places,  $r = 5$  m and 20 m for MulRan, but for CS-Wild-Places we use  $r = 10$  m and 30 m, with the 10 m threshold added to capture fine-grained PR performance. For re-ranking evaluation, we re-rank the top-20 retrieval candidates and re-compute all metrics under the new ranking.

To evaluate metric localisation, we estimate the 6-DoF pose between each query and top-candidate retrieval obtained during PR evaluation, and compare the pose estimate with the ground truth pose. To ensure a fair evaluation, we exclude PR failures (*i.e.*, candidates that do not overlap the query) from the evaluation. We report three metrics: success rate, which measures the percentage of queries registered within 2 m and  $5^\circ$  of the ground truth pose, as well as relative rotation error (RRE) and relative translation error (RTE), as defined in [19]. We refine ground truth poses with ICP to ensure accurate ground truth. Following SGV, we average RRE and RTE over *all* localisation pairs rather than successful pairs to capture the true performance of the system. Importantly, we report all metrics *without* ICP refining the pose estimates.

### B. Implementation Details

See Tab. II for dataset-specific hyperparameters. We train HOTFLoc++ on a single NVIDIA H100 GPU. HOTFLoc++ employs a lightweight version of the HOTFormerLoc [4] backbone with  $S = 3$  pyramid levels and a maximum channel size of 192. Our network has 14.8 M parameters in total, of which 1.6 M belong to the re-ranking and metric localisation heads. During training, we apply data augmentations including random point jitter, random point removal, random translations within  $\pm 5$  m, random rotations about the z-axis between  $\pm 180^\circ$ , and random occlusions up to  $45^\circ$ .

In our two-stage training protocol, we pre-train the PR head with batch size 2048 for 60 epochs, followed by 60 epochs with batch size 256 and losses  $\mathcal{L}_{rr}$ ,  $\mathcal{L}_{cm}$ , and  $\mathcal{L}_{fm}$

TABLE III: Place recognition and 6-DoF metric localisation results on CS-Wild-Places [4] baseline set.

| Method                        | Re-Ranker          | Karawatha   |             |             |             |                           |             |              | Venman      |             |             |             |                           |             |             |
|-------------------------------|--------------------|-------------|-------------|-------------|-------------|---------------------------|-------------|--------------|-------------|-------------|-------------|-------------|---------------------------|-------------|-------------|
|                               |                    | PR (10 m)   |             | PR (30 m)   |             | 6-DoF Metric Localisation |             |              | PR (10 m)   |             | PR (30 m)   |             | 6-DoF Metric Localisation |             |             |
|                               |                    | R1          | R5          | R1          | R5          | Succ.                     | RTE [m]     | RRE [°]      | R1          | R5          | R1          | R5          | Succ.                     | RTE [m]     | RRE [°]     |
| MinkLoc3Dv2 [12]              | —                  | 31.1        | 54.2        | 56.1        | 70.2        | —                         | —           | —            | 33.8        | 63.6        | 61.2        | 79.2        | —                         | —           | —           |
| EgoNN [13]                    | —                  | 34.3        | 61.4        | 60.0        | 76.2        | 43.3%                     | 7.81        | 44.64        | 37.7        | 62.3        | 59.8        | 77.4        | 31.7%                     | 11.20       | 63.69       |
| LoGG3D-Net* <sup>†</sup> [11] | —                  | 18.7        | 37.7        | 33.7        | 50.8        | <u>78.3%</u>              | <u>3.39</u> | <u>11.70</u> | 11.7        | 29.6        | 26.1        | 48.1        | <u>95.1%</u>              | <u>1.24</u> | <u>3.75</u> |
| HOTFormerLoc [4]              | —                  | 34.6        | 61.7        | 62.6        | 76.9        | —                         | —           | —            | 31.5        | 55.1        | 54.3        | 70.5        | —                         | —           | —           |
| <b>HOTFLoc++ (Ours)</b>       | —                  | <b>44.4</b> | <b>71.2</b> | <b>72.0</b> | <b>84.1</b> | <b>82.9%</b>              | <b>2.32</b> | <b>5.74</b>  | <b>38.4</b> | <b>68.1</b> | <b>65.2</b> | <b>82.1</b> | <b>96.9%</b>              | <b>0.58</b> | <b>1.47</b> |
| EgoNN [13]                    | SGV [1]            | 48.6        | 68.3        | 64.6        | 79.7        | 56.9%                     | 4.70        | 26.79        | 33.9        | 60.4        | 52.5        | 79.7        | 40.1%                     | 9.61        | 51.57       |
| LoGG3D-Net* <sup>†</sup> [11] | SGV [1]            | 28.9        | 45.1        | 45.8        | 55.3        | 81.5%                     | 2.50        | 9.18         | 34.1        | 52.4        | 64.4        | 66.7        | 97.9%                     | 0.55        | 1.99        |
| <b>HOTFLoc++ (Ours)</b>       | SGV [1]            | <b>67.5</b> | <b>82.4</b> | <b>85.9</b> | <b>89.0</b> | <b>85.9%</b>              | <b>1.70</b> | <b>3.37</b>  | <b>70.9</b> | <b>84.1</b> | <b>91.0</b> | <b>92.5</b> | <b>98.7%</b>              | <b>0.42</b> | <b>1.00</b> |
| <b>HOTFLoc++ (Ours)</b>       | <b>MSGV (Ours)</b> | <b>66.1</b> | <b>81.1</b> | <b>81.6</b> | <b>88.2</b> | <b>88.9%</b>              | <b>1.11</b> | <b>1.57</b>  | <b>77.8</b> | <b>86.1</b> | <b>93.5</b> | <b>93.9</b> | <b>99.0%</b>              | <b>0.38</b> | <b>0.85</b> |

\* Method uses 1024-dimensional global descriptors, instead of 256-dimensional.

<sup>†</sup> Method uses 0.8 m voxel downsampling instead of 0.4 m to remain tractable.

TABLE IV: Place recognition and 6-DoF metric localisation results on CS-Wild-Places [4] unseen set.

| Method                        | Re-Ranker          | QCAT        |             |             |             |                           |             |              | Samford     |             |             |             |                           |             |             |
|-------------------------------|--------------------|-------------|-------------|-------------|-------------|---------------------------|-------------|--------------|-------------|-------------|-------------|-------------|---------------------------|-------------|-------------|
|                               |                    | PR (10 m)   |             | PR (30 m)   |             | 6-DoF Metric Localisation |             |              | PR (10 m)   |             | PR (30 m)   |             | 6-DoF Metric Localisation |             |             |
|                               |                    | R1          | R5          | R1          | R5          | Succ.                     | RTE [m]     | RRE [°]      | R1          | R5          | R1          | R5          | Succ.                     | RTE [m]     | RRE [°]     |
| MinkLoc3Dv2 [12]              | —                  | 13.0        | 43.6        | <b>51.0</b> | <b>79.9</b> | —                         | —           | —            | 28.2        | 53.7        | 53.6        | 71.9        | —                         | —           | —           |
| EgoNN [13]                    | —                  | 13.5        | 37.8        | 49.4        | 67.3        | 54.6%                     | 12.41       | 50.07        | 27.4        | 51.6        | 46.5        | 65.5        | 89.8%                     | 2.75        | 10.56       |
| LoGG3D-Net* <sup>†</sup> [11] | —                  | 14.3        | 31.2        | 37.5        | 61.3        | 52.8%                     | 15.33       | <u>33.09</u> | 3.4         | 9.6         | 12.3        | 23.5        | 35.1%                     | 22.12       | 44.33       |
| HOTFormerLoc [4]              | —                  | 17.7        | 41.4        | 45.6        | 68.2        | —                         | —           | —            | 43.3        | 73.0        | 75.8        | 87.2        | —                         | —           | —           |
| <b>HOTFLoc++ (Ours)</b>       | —                  | <b>19.7</b> | <b>44.5</b> | 46.7        | 66.0        | <b>95.8%</b>              | <b>1.31</b> | <b>2.40</b>  | <b>48.4</b> | <b>79.4</b> | <b>81.4</b> | <b>89.5</b> | <b>96.3%</b>              | <b>1.56</b> | <b>1.93</b> |
| EgoNN [13]                    | SGV [1]            | 40.0        | 54.6        | 53.7        | 71.6        | 79.3%                     | 4.86        | 22.31        | 63.9        | 68.4        | 73.4        | 76.6        | 98.3%                     | 1.24        | 1.79        |
| LoGG3D-Net* <sup>†</sup> [11] | SGV [1]            | 18.5        | 36.5        | 42.5        | 64.6        | 47.2%                     | 12.61       | 31.51        | 6.2         | 13.3        | 20.8        | 28.2        | 38.6%                     | 20.72       | 32.69       |
| <b>HOTFLoc++ (Ours)</b>       | SGV [1]            | <b>61.1</b> | <b>68.8</b> | <b>71.2</b> | <b>79.8</b> | <b>98.2%</b>              | <b>0.51</b> | <b>0.78</b>  | <b>65.4</b> | <b>90.5</b> | <b>94.5</b> | <b>95.2</b> | <b>96.8%</b>              | <b>1.32</b> | <b>1.47</b> |
| <b>HOTFLoc++ (Ours)</b>       | <b>MSGV (Ours)</b> | <b>72.8</b> | <b>83.5</b> | <b>92.2</b> | <b>95.0</b> | <b>96.7%</b>              | <b>0.77</b> | <b>1.55</b>  | <b>71.6</b> | <b>94.1</b> | <b>95.3</b> | <b>96.5</b> | <b>99.1%</b>              | <b>1.17</b> | <b>0.97</b> |

enabled, where  $\lambda_{rr} = \lambda_{cm} = \lambda_{fm} = 1$ . In both stages, we reduce the initial learning rate by a factor of 10 after 40 epochs, and apply a memory-efficient sharpness-aware loss [27] after 10 epochs to encourage convergence to a flat minima. In MSGV, we sample  $\lambda_s \in \{512, 256, 128\}$  correspondences from fine to coarse levels. In our metric localisation head, we set the number of top-k coarse correspondences to  $N_c = 256$ , and point confidence threshold to  $\gamma_z = 0.05$ .

### C. Results

*CS-Wild-Places:* We compare our method with end-to-end LiDAR PR methods including MinkLoc3Dv2 [12], EgoNN [13], LoGG3D-Net [11], and HOTFormerLoc [4]. All methods produce a 256-dimensional global descriptor, except for LoGG3D-Net as we adopt the larger network used in [1] with a 1024-dimensional global descriptor. We adapt LoGG3D-Net for metric localisation via RANSAC matching on local features, mirroring the approach used in [1]. We also compare our MSGV re-ranking head with SpectralGV [1]. Tables III and IV show results for the baseline and unseen splits of CS-Wild-Places, respectively.

HOTFLoc++ excels in the challenging cross-source ground-to-aerial re-localisation setting, outperforming previous methods by a significant margin with and without re-ranking enabled. Without re-ranking, our backbone achieves a 9.4 and 12.4 percentage point (p.p.) average improvement in Recall@1 over EgoNN for the 10 m and 30 m retrieval thresholds, respectively. With SGV re-ranking enabled, this improvement increases to 19.6 p.p. and 24.6 p.p., and with MSGV it further rises to 25.5 p.p. and 29.6 p.p. over EgoNN.

Notably, our MSGV re-ranking outperforms SGV, with a significant Recall@1 improvement of up to 21.0 p.p. on QCAT. Empirically, we find that QCAT exhibits significant perceptual aliasing, causing a large number of false positive correspondences at the feature resolution used by

SGV. Our method filters out these false positives by jointly considering the geometric consistency of correspondences at different granularities, improving robustness in the presence of degraded single-resolution correspondences. Additionally, MSGV identifies higher overlap candidates for registration, reducing metric localisation error by  $\sim 2\times$  on average.

The 6-DoF metric localisation results highlight the weaknesses of keypoint-based methods in dense forests, with HOTFLoc++ achieving an average success rate of 95.9% with re-ranking enabled, compared to EgoNN's average success rate of 68.7%. This difference is largely due to how challenging it is to produce repeatable keypoints in dense forests. The cross-source nature of CS-Wild-Places also plays a significant role, as the varying densities of points captured from the ground and aerial perspectives biases keypoints towards regions that may not be well sampled from the other perspective. By contrast, the coarse-to-fine registration of HOTFLoc++ considers patch-to-patch matches, which can still produce accurate registrations under low overlap. Furthermore, our method's robust hypothesise-and-verify approach prevents erroneous patch correspondences from corrupting the registration. Our 6-DoF metric localisation approach also consistently outperforms the RANSAC-based registration used in LoGG3D-Net, with significantly better generalisation to the unseen forests, whilst requiring two orders of magnitude less runtime (Tab. VII).

*Wild-Places:* We evaluate our approach on the Wild-Places dataset in Tab. V. For place recognition, our approach consistently reports higher Recall@5 than baselines, achieving 97.8% and 99.6% on Karawatha and Venman, respectively. LoGG3D-Net maintains the highest Recall@1 across both splits, but requires a bulkier 1024-dimensional global descriptor to achieve this, as shown in [4]. Our MSGV re-ranking improves average Recall@1 by up to 21.7 p.p. and 39.6 p.p. on Karawatha and Venman, respectively. We do

TABLE V: Place recognition and 6-DoF metric localisation results on Wild-Places [17] inter-sequence protocol.

| Method                  | Re-Ranker          | Karawatha   |             |                           |             |             |         | Venman      |             |                           |             |         |             |
|-------------------------|--------------------|-------------|-------------|---------------------------|-------------|-------------|---------|-------------|-------------|---------------------------|-------------|---------|-------------|
|                         |                    | PR (3m)     |             | 6-DoF Metric Localisation |             |             | RRE [°] | PR (3m)     |             | 6-DoF Metric Localisation |             |         | RRE [°]     |
|                         |                    | R1          | R5          | Succ.                     | RTE [m]     | RRE [°]     |         | R1          | R5          | Succ.                     | RTE [m]     | RRE [°] |             |
| MinkLoc3Dv2 [12]        | —                  | 67.8        | 92.6        | —                         | —           | —           | —       | 79.8        | 96.1        | —                         | —           | —       | —           |
| EgoNN [13]              | —                  | 70.9        | 92.8        | —                         | —           | 1.14        | 10.53   | 77.2        | 95.6        | 77.3%                     | 0.90        | —       | 7.91        |
| LoGG3D-Net* [11]        | —                  | <b>74.9</b> | 92.4        | <b>96.6%</b>              | <b>0.37</b> | <b>2.34</b> | —       | 79.4        | 93.6        | <b>98.0%</b>              | <b>0.52</b> | —       | <b>2.03</b> |
| HOTFormerLoc [4]        | —                  | 69.6        | 92.2        | —                         | —           | —           | —       | <b>80.1</b> | 96.4        | —                         | —           | —       | —           |
| <b>HOTFLoc++ (Ours)</b> | —                  | 71.1        | <b>93.4</b> | 89.2%                     | 0.88        | 4.53        | —       | 79.9        | <b>96.9</b> | 95.7%                     | <b>0.52</b> | —       | 2.66        |
| EgoNN [13]              | SGV [1]            | 90.1        | 97.5        | 74.0%                     | 0.49        | 5.67        | —       | 96.6        | 99.3        | 82.2%                     | 0.37        | —       | 3.90        |
| LoGG3D-Net* [11]        | SGV [1]            | 91.6        | 97.3        | <b>97.9%</b>              | <b>0.24</b> | <b>1.06</b> | —       | <b>97.0</b> | 98.4        | <b>99.9%</b>              | <b>0.17</b> | —       | <b>0.59</b> |
| <b>HOTFLoc++ (Ours)</b> | SGV [1]            | <b>91.7</b> | <b>98.0</b> | 96.6%                     | 0.38        | 2.49        | —       | 95.9        | <b>99.6</b> | 99.4%                     | 0.29        | —       | 1.57        |
| <b>HOTFLoc++ (Ours)</b> | <b>MSGV (Ours)</b> | 89.4        | 97.8        | 96.6%                     | 0.39        | 2.39        | —       | 94.0        | <b>99.6</b> | 99.6%                     | 0.28        | —       | 1.28        |

\* Method uses 1024-dimensional global descriptors, instead of 256-dimensional.

TABLE VI: Place recognition and 6-DoF metric localisation results on MulRan [26].

| Method                   | Sejong 02   |             |             |             |                   |             | DCC 02      |             |             |             |                   |             | Riverside 02 |             |             |             |                   |              |
|--------------------------|-------------|-------------|-------------|-------------|-------------------|-------------|-------------|-------------|-------------|-------------|-------------------|-------------|--------------|-------------|-------------|-------------|-------------------|--------------|
|                          | PR (5 m)    |             | PR (20 m)   |             | 6-DoF Metric Loc. |             | PR (5 m)    |             | PR (20 m)   |             | 6-DoF Metric Loc. |             | PR (5 m)     |             | PR (20 m)   |             | 6-DoF Metric Loc. |              |
|                          | R1          | R5          | R1          | R5          | Succ.             | RTE         | R1          | R5          | R1          | R5          | Succ.             | RTE         | R1           | R5          | R1          | R5          | Succ.             | RTE          |
| EgoNN [13]               | <b>98.2</b> | <b>99.7</b> | <b>99.2</b> | <b>99.8</b> | 99.8%             | 0.20        | 68.1        | 86.6        | 89.9        | 94.5        | 97.1%             | 0.62        | <b>72.9</b>  | 86.2        | 84.1        | 91.0        | 98.4%             | <b>0.27</b>  |
| LoGG3D-Net* [11]         | 97.3        | <b>99.7</b> | 98.6        | <b>99.8</b> | <b>99.9%</b>      | <b>0.18</b> | 69.1        | 88.9        | 91.5        | 95.4        | <b>98.6%</b>      | <b>0.25</b> | <b>0.40</b>  | 69.2        | 89.7        | 85.6        | 93.3              | <b>98.5%</b> |
| HOTFormerLoc [4]         | 96.9        | 99.3        | <b>99.2</b> | 99.7        | —                 | —           | <b>69.4</b> | 93.2        | <b>95.4</b> | 97.1        | —                 | —           | —            | 66.0        | 91.0        | 88.2        | 95.3              | —            |
| <b>HOTFLoc++</b>         | 96.8        | 99.2        | 99.0        | 99.5        | 97.0%             | 0.43        | 67.8        | <b>94.5</b> | <b>95.4</b> | <b>98.4</b> | 88.7%             | 1.20        | 3.68         | 67.3        | 90.5        | 89.9        | 96.3              | 88.5%        |
| <b>HOTFLoc++†</b>        | 97.0        | 99.3        | <b>99.2</b> | 99.7        | 98.8%             | 0.23        | <b>68.1</b> | 93.5        | <b>95.4</b> | 97.7        | 96.6%             | 0.42        | 1.12         | 69.2        | <b>92.7</b> | <b>92.3</b> | <b>97.0</b>       | 96.2%        |
| EgoNN [13] (SGV)         | 97.0        | 99.0        | 98.2        | <b>99.9</b> | 99.7%             | 0.19        | 74.6        | 93.2        | 97.4        | 97.7        | <b>99.3%</b>      | <b>0.18</b> | 0.55         | 80.0        | 90.5        | 87.1        | 93.8              | <b>99.5%</b> |
| LoGG3D-Net* [11] (SGV)   | <b>98.8</b> | <b>99.9</b> | 99.4        | <b>99.9</b> | <b>99.9%</b>      | <b>0.17</b> | 73.0        | 91.2        | 96.7        | 96.7        | <b>99.3%</b>      | 0.20        | 0.39         | <b>89.2</b> | 96.6        | 95.1        | 98.5              | 99.2%        |
| <b>HOTFLoc++</b> (SGV)   | 94.2        | 99.6        | <b>99.6</b> | <b>99.9</b> | 96.9%             | 0.39        | 71.0        | <b>96.1</b> | <b>99.3</b> | <b>99.7</b> | 91.8%             | 0.96        | 4.95         | 76.3        | 95.3        | 95.7        | 97.6              | 89.3%        |
| <b>HOTFLoc++†</b> (SGV)  | 95.1        | 99.8        | 99.5        | <b>99.9</b> | 98.9%             | 0.19        | 71.0        | 95.8        | 98.7        | <b>99.7</b> | 98.0%             | 0.22        | <b>0.36</b>  | 79.6        | <b>97.4</b> | <b>96.8</b> | <b>99.1</b>       | 97.0%        |
| <b>HOTFLoc++</b> (MSGV)  | 93.2        | 99.5        | 99.2        | <b>99.8</b> | 95.3%             | 0.46        | 68.1        | <b>95.8</b> | 97.7        | <b>99.0</b> | 90.4%             | 1.19        | 4.24         | 75.5        | 95.3        | <b>96.8</b> | 98.3              | 88.5%        |
| <b>HOTFLoc++†</b> (MSGV) | 94.4        | 99.5        | 99.2        | 99.8        | 98.1%             | 0.28        | 72.3        | 94.1        | 96.7        | 97.7        | 97.2%             | 0.28        | 1.57         | 77.0        | 96.3        | <b>96.8</b> | 98.7              | 97.7%        |

TABLE VII: Runtime analysis on CS-Wild-Places [4].

| Method                  | Feat. Extract. |            | Re-Ranking |            | Metric Loc. |            | Total       |
|-------------------------|----------------|------------|------------|------------|-------------|------------|-------------|
|                         | mean           | std        | mean       | std        | mean        | std        |             |
| EgoNN (SGV)             | <b>19.9</b>    | <b>4.4</b> | <b>1.2</b> | <b>1.3</b> | <b>7.6</b>  | <b>1.0</b> | <b>28.7</b> |
| LoGG3D-Net* (SGV)       | 58.0           | 7.1        | 460.0      | 300.9      | 8862.1      | 5739.4     | 9380.0      |
| <b>HOTFLoc++</b> (SGV)  | 36.4           | 5.8        | 22.7       | 2.4        | 33.5        | <b>0.3</b> | 92.5        |
| <b>HOTFLoc++</b> (MSGV) | 36.4           | 5.8        | 33.3       | <b>1.3</b> | 33.5        | <b>0.3</b> | 103.2       |

\* Runtime is reported in ms.

† Method uses 0.8 m voxel downsampling instead of 0.4 m to remain tractable.

observe SGV achieves 2.1 p.p. higher Recall@1 on average with our backbone, but we argue this small trade-off on single-source data is justified for the improved robustness seen in cross-source environments.

For 6-DoF metric localisation, LoGG3D-Net achieves the best average success rate before and after re-ranking. This is not unexpected as it relies on RANSAC feature matching between the full set of local features, which takes 1.5 s on average for Wild-Places with a mean submap size of 17 k points. In contrast, our HOTFLoc++ achieves comparable RTE and RRE with a total runtime of 101 ms on the same hardware, with only 34.7 ms of that time required for metric localisation. See Sec. IV-D for further runtime comparisons. Compared with keypoint-based re-localisation, the advantages of HOTFLoc++ are evident. It achieves an average success rate of 98.0% across all splits: an improvement of 20.2 p.p. over EgoNN.

**MulRan:** We report results on the MulRan dataset in Tab. VI. Note we also report results for a deeper version of our network with  $S = 4$  HOTFormer levels (denoted HOTFLoc++†), as we empirically find that MulRan’s urban setting benefits from coarser features than in forests. For LoGG3D-Net, we utilise the pre-trained weights from [1].

While our primary focus is on unstructured forest environments, we demonstrate comparable performance with existing methods in the urban environments of MulRan. Consistent with the findings in Wild-Places, our HOTFLoc++ with MSGV achieves the highest overall Recall@5 with an average of 96.9% and 99.0% on the 5 m and 20 m

TABLE VIII: Impact of joint training on place recognition.

| $\mathcal{L}_{pr}$ | $\mathcal{L}_{rr}$ | $\mathcal{L}_{cm}$ | $\mathcal{L}_{fm}$ | CS-Wild-Places | Wild-Places | MulRan      |
|--------------------|--------------------|--------------------|--------------------|----------------|-------------|-------------|
| ✓                  | ✓                  | ✓                  | ✓                  | 31.3           | 72.9        | 82.1        |
| ✓                  | ✓                  | ✓                  | ✓                  | 32.0           | 72.0        | 82.3        |
| ✓                  | ✓                  | ✓                  | ✓                  | 37.7           | 73.6        | 82.4        |
| ✓                  | ✓                  | ✓                  | ✓                  | <b>38.4</b>    | <b>75.5</b> | <b>83.3</b> |

Values indicate mean R1 for smallest retrieval threshold *without* re-ranking.

retrieval thresholds, respectively. Our method also achieves high Recall@1 for the 20 m retrieval threshold, with an average of 94.8% and 97.9% before and after re-ranking, respectively. Furthermore, our HOTFLoc++† model achieves comparable metric localisation performance to EgoNN and LoGG3D-Net, with an average success rate of 97.7%.

Interestingly, on the saturated Sejong 02 sequence, both EgoNN and our method exhibit *worse* Recall@1 for the 5 m threshold after re-ranking with both SGV and MSGV. Upon investigation, these failures primarily occur in a specific region with high feature ambiguity at all scales, where both EgoNN and HOTFLoc++ identify clusters of geometrically consistent but *incorrect* correspondences, which is enough to compromise geometric consistency-based re-rankers. Developing re-ranking solutions that can better handle such ambiguities is a potential direction for future research.

#### D. Runtime Analysis

We conduct a runtime analysis of 6-DoF re-localisation methods in Tab. VII. Our hardware setup includes a NVIDIA H100 GPU and Intel 8452Y CPU, which we limit to use 12 cores. EgoNN achieves the fastest overall runtime of 28.7 ms, which we attribute to its lightweight CNN backbone and sparse keypoint-based approach. Whilst efficient, we have demonstrated in Tabs. III to V that this localisation approach struggles in forest environments. Our HOTFLoc++ manages a competitive runtime of 103.2 ms, allowing for  $\sim 10$  Hz operation. Notably, our RANSAC-free metric localisation head runs more than two orders of magnitude faster than



TABLE IX: Ablation of num. feature scales used in MSGV.

| Num. Scales  | CS-Wild-Places | Wild-Places | MulRan      |
|--------------|----------------|-------------|-------------|
| 1 (fine)     | 67.8           | 90.6        | 75.6        |
| 2 (fine+mid) | 69.2           | <b>91.7</b> | 77.8        |
| 3            | <b>72.1</b>    | 91.2        | <b>80.7</b> |

Values indicate mean R1 for smallest retrieval threshold.

LoGG3D-Net with RANSAC, whilst achieving comparable or better registration results in all datasets.

### E. Ablation Study

*Joint Training:* In Tab. VIII we evaluate the impact that our joint training protocol has on the place recognition performance of HOTFLoc++, *without* re-ranking enabled at inference. A key finding is that our re-ranking and metric localisation losses have a positive impact on PR performance across most datasets. The largest individual increase is brought by  $\mathcal{L}_{cm}$  and  $\mathcal{L}_{fm}$  with an average Recall@1 improvement of 2.5 p.p., while enabling all losses produces an average improvement of 3.6 p.p.

Indeed, these losses provide beneficial constraints on the distribution of local features during training, as both losses guide the network to extract distinctive features which are invariant to rigid transformations and thus easier to match. This finding matches the observations in [11] that consistent local features tend to improve global descriptor repeatability.

*Multi-Scale Geometric Verification:* We assess the improvement gained by using multiple feature scales with our MSGV re-ranker in Tab. IX. Across all datasets, using at least 2 resolutions improves performance compared to single-resolution correspondences. Our method achieves the best performance on CS-Wild-Places and MulRan when using all 3 feature granularities, with average Recall@1 improvements of 4.3 p.p. and 5.1 p.p., respectively.

### V. CONCLUSION

This paper introduces HOTFLoc++, a unified framework trained end-to-end for LiDAR place recognition, re-ranking, and 6-DoF metric localisation. We propose a learnable multi-scale geometric verification module that improves robustness in the presence of degraded single-resolution correspondences, demonstrating significant improvements in cross-source forest environments. Our framework presents a coarse-to-fine registration approach that achieves comparable performance to RANSAC-based approaches with a runtime improvement of two orders of magnitude. Furthermore, our experiments demonstrate the complementary nature of our joint training approach, with our re-ranking and metric localisation losses contributing to higher place recognition performance. In future work, we will incorporate multi-modality to further improve robustness in challenging environments.

### REFERENCES

- [1] K. Vidanapathirana, P. Moghadam, S. Sridharan, and C. Fookes, "Spectral Geometric Verification: Re-Ranking Point Cloud Retrieval for Metric Localization," *IEEE Robot. Automat. Lett.*, vol. 8, no. 5, pp. 2494–2501, May 2023.
- [2] T. Guan, A. Muthuselvan, M. Hoover, X. Wang, J. Liang, A. J. Sathyamoorthy, D. Conover, and D. Manocha, "CrossLoc3D: Aerial-Ground Cross-Source 3D Place Recognition," *Proc. IEEE/CVF Int. Conf. Comput. Vis.*, pp. 11 301–11 310, 2023.
- [3] L. Carvalho de Lima, E. Griffiths, M. Haghighat, S. Denman, C. Fookes, P. Borges, M. Brunig, and M. Ramezani, "Online 6DoF Global Localisation in Forests using Semantically-Guided Re-Localisation and Cross-View Factor-Graph Optimisation," in *Proc. IEEE/RSJ Int. Conf. Intell. Robots Syst.*, 2025.
- [4] E. Griffiths, M. Haghighat, S. Denman, C. Fookes, and M. Ramezani, "HOTFormerLoc: Hierarchical Octree Transformer for Versatile LiDAR Place Recognition Across Ground and Aerial Views," in *Proc. IEEE/CVF Conf. Comput. Vis. Pattern Recognit.*, 2025, pp. 6648–6658.
- [5] G. Kim and A. Kim, "Scan Context: Egocentric Spatial Descriptor for Place Recognition Within 3D Point Cloud Map," in *Proc. IEEE/RSJ Int. Conf. Intell. Robots Syst.*, 2018, pp. 4802–4809.
- [6] X. Xu, S. Lu, J. Wu, H. Lu, Q. Zhu, Y. Liao, R. Xiong, and Y. Wang, "RING++: Roto-Translation Invariant Gram for Global Localization on a Sparse Scan Map," *IEEE Trans. Robot.*, vol. 39, no. 6, pp. 4616–4635, Dec. 2023.
- [7] M. A. Uy and G. H. Lee, "PointNetVLAD: Deep Point Cloud Based Retrieval for Large-Scale Place Recognition," in *Proc. IEEE/CVF Conf. Comput. Vis. Pattern Recognit.*, June 2018, pp. 4470–4479.
- [8] J. Du, R. Wang, and D. Cremers, "DH3D: Deep Hierarchical 3D Descriptors for Robust Large-Scale 6DoF Relocalization," in *Proc. Eur. Conf. Comput. Vis.*, 2020, pp. 744–762.
- [9] J. Komorowski, "MinkLoc3D: Point Cloud Based Large-Scale Place Recognition," in *Proc. IEEE Winter Conf. Appl. Comput. Vis.*, Jan. 2021, pp. 1789–1798.
- [10] D. Cattaneo, M. Vaghi, and A. Valada, "LCDNet: Deep Loop Closure Detection and Point Cloud Registration for LiDAR SLAM," *IEEE Trans. Robot.*, vol. 38, no. 4, pp. 2074–2093, Aug. 2022.
- [11] K. Vidanapathirana, M. Ramezani, P. Moghadam, S. Sridharan, and C. Fookes, "LoGG3D-Net: Locally Guided Global Descriptor Learning for 3D Place Recognition," in *Proc. IEEE Int. Conf. Robot. Automat.*, 2022, pp. 2215–2221.
- [12] J. Komorowski, "Improving Point Cloud Based Place Recognition with Ranking-based Loss and Large Batch Training," in *26th Int. Conf. Pattern Recognit.* IEEE, 2022, pp. 3699–3705.
- [13] J. Komorowski, M. Wyszczanska, and T. Trzcinski, "EgoNN: Egocentric Neural Network for Point Cloud Based 6DoF Relocalization at the City Scale," *IEEE Robot. Automat. Lett.*, vol. 7, no. 2, pp. 722–729, Apr. 2022.
- [14] L. Hui, H. Yang, M. Cheng, J. Xie, and J. Yang, "Pyramid Point Cloud Transformer for Large-Scale Place Recognition," in *Proc. IEEE/CVF Int. Conf. Comput. Vis.*, 2021, pp. 6098–6107.
- [15] T.-X. Xu, Y.-C. Guo, Z. Li, G. Yu, Y.-K. Lai, and S.-H. Zhang, "TransLoc3D: Point cloud based large-scale place recognition using adaptive receptive fields," *Commun. Inf. Syst.*, vol. 23, no. 1, pp. 57–83, 2023.
- [16] R. G. Goswami, N. Patel, P. Krishnamurthy, and F. Khorrami, "SALSA: Swift Adaptive Lightweight Self-Attention for Enhanced LiDAR Place Recognition," *IEEE Robot. Autom. Lett.*, vol. 9, no. 10, pp. 8242–8249, Oct. 2024.
- [17] J. Knights, K. Vidanapathirana, M. Ramezani, S. Sridharan, C. Fookes, and P. Moghadam, "Wild-Places: A Large-Scale Dataset for Lidar Place Recognition in Unstructured Natural Environments," in *Proc. IEEE Int. Conf. Robot. Automat.*, 2023, pp. 11 322–11 328.
- [18] M. A. Fischler and R. C. Bolles, "Random sample consensus: A paradigm for model fitting with applications to image analysis and automated cartography," *Commun. ACM*, vol. 24, no. 6, pp. 381–395, June 1981.
- [19] X. Bai, Z. Luo, L. Zhou, H. Chen, L. Li, Z. Hu, H. Fu, and C.-L. Tai, "PointDSC: Robust Point Cloud Registration using Deep Spatial Consistency," in *Proc. IEEE/CVF Conf. Comput. Vis. Pattern Recognit.*, June 2021, pp. 15 854–15 864.
- [20] H. Yu, F. Li, M. Saleh, B. Busam, and S. Ilic, "CoFiNet: Reliable Coarse-to-fine Correspondences for Robust PointCloud Registration," in *Proc. Adv. Neural Inf. Process. Syst.*, vol. 34, 2021, pp. 23 872–23 884.
- [21] Z. Qin, H. Yu, C. Wang, Y. Guo, Y. Peng, S. Ilic, D. Hu, and K. Xu, "GeoTransformer: Fast and Robust Point Cloud Registration With Geometric Transformer," *IEEE Trans. Pattern Anal. Machine Intell.*, vol. 45, no. 8, pp. 9806–9821, Aug. 2023.
- [22] J. Knights, S. Hausler, S. Sridharan, C. Fookes, and P. Moghadam, "GeoAdapt: Self-Supervised Test-Time Adaptation in LiDAR Place Recognition Using Geometric Priors," *IEEE Robot. Automat. Lett.*, vol. 9, no. 1, pp. 915–922, Jan. 2024.



- [23] M. Leordeanu and M. Hebert, "A spectral technique for correspondence problems using pairwise constraints," in *Proc. 10th IEEE Int. Conf. Comput. Vis.*, vol. 2, Oct. 2005, pp. 1482–1489.
- [24] P.-E. Sarlin, D. DeTone, T. Malisiewicz, and A. Rabinovich, "Super-Glue: Learning Feature Matching With Graph Neural Networks," in *Proc. IEEE/CVF Conf. Comput. Vis. Pattern Recognit.*, June 2020, pp. 4937–4946.
- [25] A. Hermans, L. Beyer, and B. Leibe, "In Defense of the Triplet Loss for Person Re-Identification," Nov. 2017, arXiv:1703.07737 [cs].
- [26] G. Kim, Y. S. Park, Y. Cho, J. Jeong, and A. Kim, "MulRan: Multimodal Range Dataset for Urban Place Recognition," in *Proc. IEEE Int. Conf. Robot. Automat.*, 2020, pp. 6246–6253.
- [27] J. Du, D. Zhou, J. Feng, V. Tan, and J. T. Zhou, "Sharpness-Aware Training for Free," *Proc. Adv. Neural Inf. Process. Syst.*, Dec. 2022.